A Hybrid CBPWM Scheme for Single-Phase Three-Level Converters

Shunliang Wang[*], Wensheng Song[†], Xiaoyun Feng[**], and Rongjun Ding[*]

[*],[†]Key Lab of Magnetic Suspension Technology and Maglev Vehicle, Ministry of Education, Department of
Electrical Engineering, Southwest Jiaotong University, Chengdu, China
[**]State Key Laboratory of Traction Power, Southwest Jiaotong University, Chengdu, China

Abstract

A novel hybrid carrier-based pulse width modulation (CBPWM) scheme that combines unipolar and dipolar modulations is proposed for single-phase three-level rectifiers, which are widely applied in railway traction drive systems. The proposed CBPWM method can satisfy the volt-second balancing principle in the complete modulation index region through overmodulation compensation. The modulation scheme features two modulation modes: unipolar and dipolar. The operation range limits of these modulation modes can be modified by changing the separation coefficient. In comparison with the traditional unipolar CBPWM, the proposed hybrid CBPWM scheme can provide advantageous features, such as lower high-order harmonic distortion of the line current and better utilization of switching frequency. The separation coefficient value is optimized to achieve the maximum utilization of these advantages. The experimental results verify the feasibility and effectiveness of the proposed hybrid CBPWM scheme.

Key words: CBPWM, Dipolar, High-order harmonics, Switching frequency, Single-phase three-level rectifier, Unipolar

I. INTRODUCTION

Single-phase three-level neutral point clamped (NPC) converters as grid-side converters have been widely used in various applications, such as in solar grid-connected inverters [1]-[3], uninterruptible power supplies (UPS) [4], power factor correction (PFC) [5], [6], and AC electric railway traction drive systems [7]-[9]. High-order harmonics can adversely affect converters and power supply systems. The high-order harmonics caused by grid-side converters may result in overvoltage, overheating, electromagnetic interference (EMI), and harmonic resonance in electric railway traction power systems and distributed generation systems [8], [10]-[14]. A resonance accident caused by high-order harmonics occurred in the China Beijing–Shanghai high-speed railway in January 9th, 2011 and resulted in a high amplitude peak voltage and arrester breakdown [15]. Minimal high-order harmonics caused by grid-side converters equate to minimal damage. The higher

frequency of high-order harmonics, the more easier to filter.

To suppress harmonics, LC or LCL filters, which are installed in UPS and PFC converters, are widely used to mitigate high-order harmonics [5], [16]-[19]. Various types of filters are installed in traction power supply systems to deal with typical harmonic distortions [10], [12]. These methods require additional filter devices. Optimal modulation algorithms in converter control systems are viewed as alternative solutions to suppress high-order harmonics as they do not require additional hardware devices. Selective harmonic elimination pulse width modulation (SHEPWM) can generally eliminate a number of unwanted harmonics in the pulse voltage of converters [20]-[22]. However, it requires numerous complicated calculations and digital memory resources. The SHEPWM processes applied in three-level and multi-level converters are also more difficult than those applied in two-level converters.

The pulse voltage under the unipolar carrier-based pulse width modulation (CBPWM) scheme consists of two voltage levels in one switching cycle. The conventional unipolar CBPWM is widely used in single-phase three-level converters because of its simplicity [7], [8], [23]. By contrast, single-phase three-level space vector pulse width modulation (SVPWM) has

Fig. 1. Topology of a single-phase three-level NPC rectifier.

G_{i1}	G_{i2}	G_{i3}	G_{i4}	S_i
1	1	0	0	1
0	1	1	0	0
0	0	1	1	−1
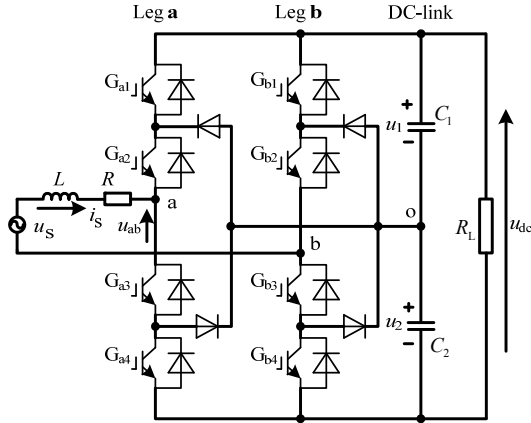
Fig. 2. Simplified control system structure of the adopted converter.

been reported for the converters in [9], [24], [25]. The performance of SVPWM is equivalent to that of the conventional unipolar CBPWM [9]. The high-order harmonics caused by these modulation algorithms are mainly distributed around the switching frequency or double switching frequency. In the dipolar CBPWM scheme, the switching signal of each leg consists of three states (1 0 −1) in one switching cycle. The dipolar modulation technique has been used in three-phase matrix and NPC converters [25], [26]. However, the characteristics of the high-order harmonics of dipolar modulation have yet to be analyzed, and this dipolar modulation method cannot be directly applied in single-phase three-level converters.

In this study, dipolar modulation is applied in a single-phase three-level converter. Combining the advantages of unipolar and dipolar modulations, we propose a simple hybrid CBPWM scheme for single-phase three-level converters. The characteristics of the high-order harmonics of the proposed hybrid CBPWM scheme and those of the traditional unipolar CBPWM scheme are compared and verified.

II. SYSTEM CONFIGURATION

Fig. 1 shows the topology of a single-phase three-level NPC rectifier. In this figure, u_s and i_s denote the main voltage and line current, respectively; R and L represent the internal resistance and inductance of the grid-side inductor, respectively; C_1 and C_2 denote the upper and lower DC-link capacitances, respectively; R_L denotes the equivalent load; and u_{dc} denotes the DC-link voltage value.

Both G_{ai} and G_{bi} ($i = 1, 2, 3, 4$) represent the drive signals for the switching devices in legs **a** and **b**, respectively. These drive signals can be defined as

$$G_{ai} = \begin{cases} 1 & G_{ai} \text{ on-state} \\ 0 & G_{ai} \text{ off-state} \end{cases} \quad (1)$$

$$G_{bi} = \begin{cases} 1 & G_{bi} \text{ on-state} \\ 0 & G_{bi} \text{ off-state} \end{cases} \quad (2)$$

S_a and S_b denote the idealized switching functions of legs **a** and **b**, respectively. The relationship between S_i and G_{ij} ($i = $ a, b; $j = 1, 2, 3, 4$) is shown in Table I. The input voltage u_{ab} of the adopted rectifier is expressed as

$$u_{ab} = u_{ao} - u_{bo} = \frac{S_a - S_b}{2}(u_1 + u_2) + \frac{S_a^2 - S_b^2}{2}(u_1 - u_2) \quad (3)$$

The states of S_a and S_b are obtained from the modulation algorithm. The reference signal u_r of the modulation algorithm is the output of the control algorithm. The simplified control system structure of the adopted converter is shown in Fig. 2.

III. MODULATION SCHEMES

The ranges of the normalized modulation reference signal u_r can be divided into the following four regions:
(1) region I: $0.5 < u_r \leq 1$
(2) region II: $0 < u_r \leq 0.5$
(3) region III: $−0.5 < u_r \leq 0$
(4) region IV: $−1 < u_r \leq −0.5$
Assuming that the switching frequency f_s is significantly higher than the modulation signal frequency, then u_r can be considered as a constant in each switching cycle.

A. Traditional Unipolar CBPWM

u_{ra} and u_{rb} denote the modulation reference signals of legs **a** and **b**, respectively, and satisfy

$$\begin{cases} u_{ra} = u_r \\ u_{rb} = -u_r \end{cases} \quad (4)$$

In a traditional single-phase three-level unipolar CBPWM algorithm, two triangle carriers (C_+ and $C_−$) and modulating signals are compared to generate the switching function states and drive pulses of an NPC converter. The principle of the unipolar CBPWM algorithm can be defined as
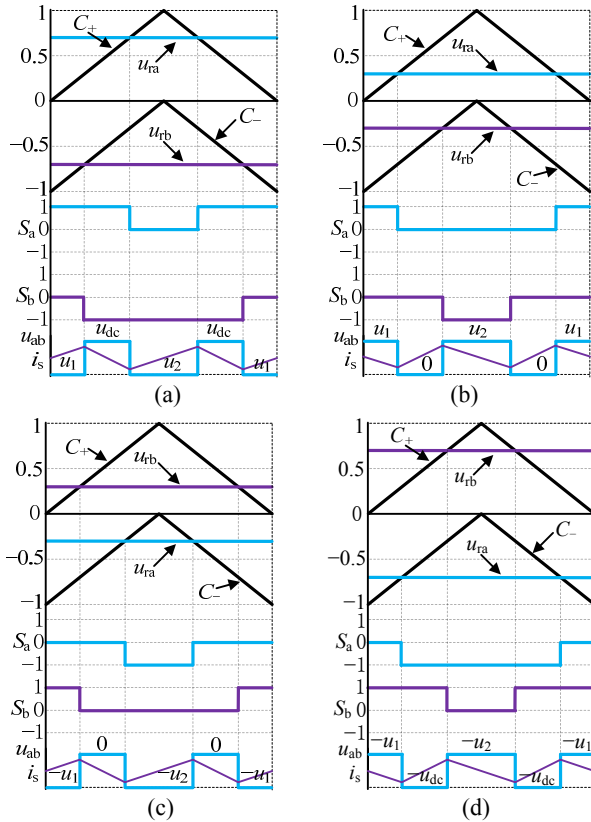
Fig. 3. Traditional unipolar CBPWM algorithm in one switching cycle T_s. (a) Region I. (b) Region II. (c) Region III. (d) Region IV.
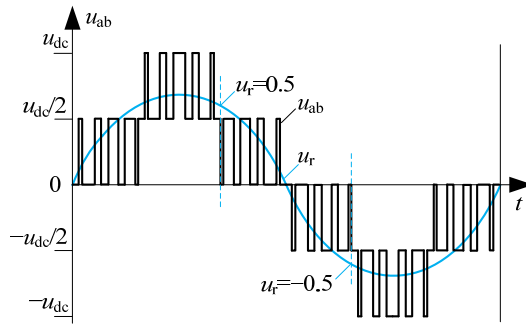

Fig. 4. Traditional unipolar CBPWM algorithm in a complete modulation cycle.

$$S_i = \begin{cases} 1 & u_{ri} \geq C_+ \\ 0 & C_- < u_{ri} < C_+ \qquad (i=\text{a, b}) \\ -1 & u_{ri} \leq C_- \end{cases} \qquad (5)$$

The switching function of each leg in the adopted unipolar CBPWM algorithm consists of state 0 and another state (1 or −1) in one switching cycle. Fig. 3 shows a traditional single-phase three-level unipolar CBPWM algorithm in one switching cycle T_s when u_r lies in four regions. The input voltage u_{ab} also comprises two voltage levels in one switching cycle. As shown in Fig. 4, u_{ab} is the waveform in a complete modulation cycle, and u_{ab} is an approximate sinusoidal pulse waveform for obtaining good high-order harmonic
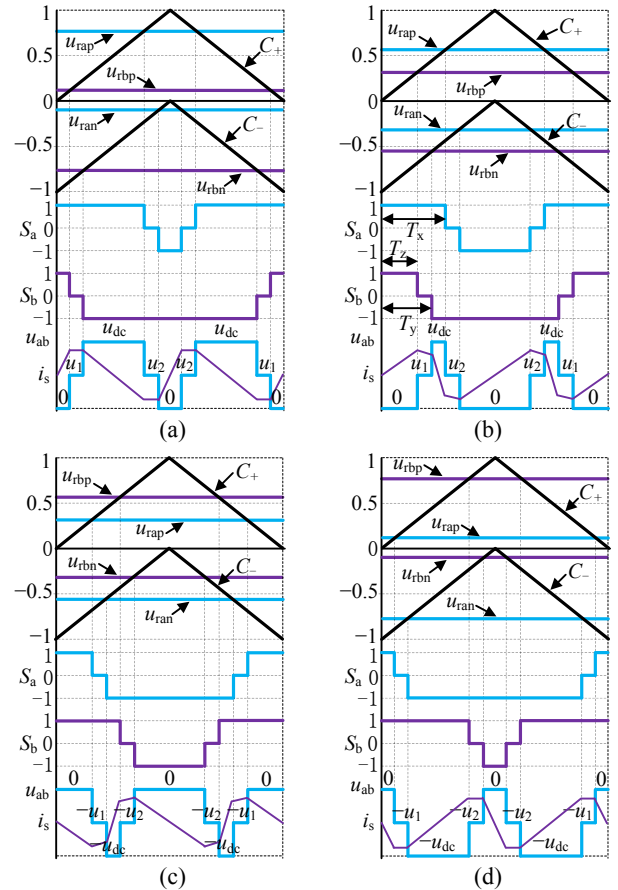

Fig. 5. Proposed single-phase three-level dipolar CBPWM algorithm in one switching cycle T_s. (a) Region I. (b) Region II. (c) Region III. (d) Region IV.

characteristics. As indicated in the diagram of current i_s in Fig. 3, the current i_s changes with the voltage u_{ab} level step, and the high-order harmonics caused by the unipolar CBPWM are mainly distributed around the double switching frequency.

B. Dipolar CBPWM

Fig. 5 shows the single-phase three-level dipolar CBPWM algorithm designed in this work. u_{rap} and u_{rbp} denote the positive modulation signals for legs **a** and **b**, respectively; u_{ran} and u_{rbn} denote the negative modulation signals for legs **a** and **b**, respectively; and λ refers to the separation coefficient with the range $0 < \lambda < 1$ and satisfies

$$\begin{cases} u_{rip} = \dfrac{u_{ri}}{2} + \lambda \\ u_{rin} = \dfrac{u_{ri}}{2} - \lambda \end{cases} \qquad (i = \text{a, b}) \qquad (6)$$

The principle of the dipolar CBPWM algorithm can be expressed as

$$S_i = \begin{cases} 1 & u_{rip} \geq C_+ \text{ and } u_{rin} \geq C_- \\ 0 & u_{rip} \geq C_+ \text{ and } u_{rin} < C_-, \\ & \text{ or } u_{rip} < C_+ \text{ and } u_{rin} \geq C_- \\ -1 & u_{rip} < C_+ \text{ and } u_{rin} < C_- \end{cases} \qquad (i=\text{a, b}) \qquad (7)$$

TABLE II
SWITCHING STATE OF EACH LEG (i = a, b)

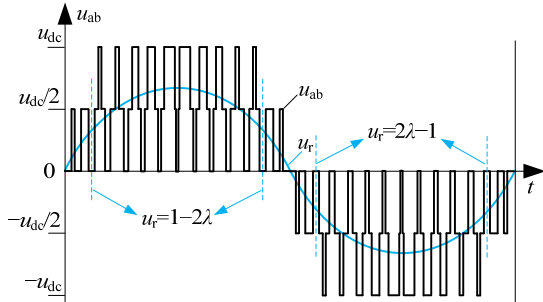| Proposed Dipolar CBPWM					Traditional Unipolar CBPWM				
S_i	G_{i1}	G_{i2}	G_{i3}	G_{i4}	S_i	G_{i1}	G_{i2}	G_{i3}	G_{i4}
1	1	1	0	0	**1**	1	1	0	0
0	0	1	1	0	**0**	0	1	1	0
−1	0	0	1	1	**1**	1	1	0	0
0	0	1	1	0					
1	1	1	0	0					

Fig. 6. Dipolar CBPWM algorithm in a complete modulation cycle.

Modulation depth m is the amplitude of the modulation signal u_r. To prevent modulation signals from entering the overmodulation region, the separation coefficient λ should meet Equ. (8).

$$\frac{m}{2} + \lambda \leq 1 \tag{8}$$

As shown in Fig. 3, the state sequence of switching functions S_a and S_b under the unipolar CBPWM scheme is $1 \to 0 \to 1$ or $0 \to -1 \to 0$ in one switching cycle. By contrast, Fig. 5 shows that the state sequence of switching functions S_a and S_b under the dipolar CBPWM scheme is $1 \to 0 \to -1 \to 0 \to 1$ in one switching cycle. Table II shows the states of the switching devices of the proposed dipolar CBPWM and traditional unipolar CBPWM ($1 \to 0 \to 1$ as an example) schemes in one switching cycle T_s. Turning on and off actions occur for half of the switching devices in one switching cycle under the unipolar CBPWM scheme. No turning action occurs for switching devices G_{i2} and G_{i4} when the sequence is $1 \to 0 \to 1$. Similarly, no turning action occurs for switching devices G_{i1} and G_{i3} when the sequence is $0 \to -1 \to 0$. However, under the dipolar CBPWM scheme, turning on and off actions occur for each switching device in one switching cycle. Moreover, the desired switching frequency does not increase. However, the total number of switching commutations is twice that under the unipolar CBPWM scheme.

Assuming that $u_1 = u_2 = 0.5u_{dc}$. T_1 is defined as the duty time of state $u_{ab} = u_{dc}$, $T_{0.5}$ is the duty time of state $u_{ab} = 0.5u_{dc}$, T_0 is the duty time of state $u_{ab} = 0$, $T_{-0.5}$ is the duty time of state $u_{ab} = -0.5u_{dc}$, and T_{-1} is the duty time of state $u_{ab} = -u_{dc}$. When u_r lies in region II, solving the same triangle as that in Fig. 5(b) yields

$$\begin{cases} \dfrac{T_x}{T_s/2} = \dfrac{u_r/2 + \lambda}{1} \\ \dfrac{T_y}{T_s/2} = \dfrac{1 - u_r/2 - \lambda}{1} \\ \dfrac{T_z}{T_s/2} = \dfrac{-u_r/2 + \lambda}{1} \end{cases} \tag{9}$$

where the lengths of T_x, T_y, and T_z are shown in Fig. 5(b).

Thus, in region II, T_1, $T_{0.5}$, and T_0 can be deduced from Equ. (9) and Fig. 5(b) as

$$\begin{cases} T_1 = 2(T_x - T_y) = (u_r + 2\lambda - 1)T_s \\ T_{0.5} = 4(T_y - T_z) = (2 - 4\lambda)T_s \\ T_0 = T_s - (T_1 + T_{0.5}) = (-u_r + 2\lambda)T_s \end{cases} \tag{10}$$

V_r is the average reference voltage, and V_{ab} is the average value of voltage u_{ab} in one switching cycle. V_r is equal to $u_r T_s u_{dc}$. When u_r lies in region II, V_{ab} can be expressed as Equ. (11). When u_r is in the other three regions, the same $V_{ab} = V_r$ can be deduced. Thus, the dipolar modulation meets the volt-second balance principle.

$$\begin{aligned} V_{ab} &= T_1 u_{dc} + 0.5T_{0.5}u_{dc} \\ &= (u_r + 2\lambda - 1)T_s u_{dc} + 0.5(2 - 4\lambda)T_s u_{dc} \\ &= u_r T_s u_{dc} = V_r \end{aligned} \tag{11}$$

Fig. 5(b) shows that if $T_x < T_y$, then voltage u_{ab} in region II and region III is composed of two voltage levels during one switching cycle. By solving the similar triangle in Fig. 5(b) on the basis of Equ. (9), the range of u_r can be expressed as

$$|u_r| < |1 - 2\lambda| \tag{12}$$

The waveform of u_{ab} in a complete modulation cycle is depicted in Fig. 6. In Fig. 6, u_{ab} presents a terrible sinusoidal pulse waveform. When u_r does not satisfy Equ. (12), the variation rate of current i_s with the voltage u_{ab} level step is larger than that under the unipolar CBPWM scheme in the comparison of the diagrams of current i_s in Fig. 5 and Fig. 3. Thus, the dipolar CBPWM scheme achieves worse high-order harmonic characteristics compared with the unipolar CBPWM scheme.

C. Hybrid CBPWM

To improve the utilization of switching frequency and achieve good high-order harmonic characteristics, we propose a hybrid CBPWM scheme, which is based on the dipolar and unipolar CBPWM schemes. According to the region of modulation signal u_r, the hybrid CBPWM scheme is divided into unipolar and dipolar modes.

When the voltage u_{ab} consists of two voltage levels in each region, the hybrid CBPWM scheme is similar to the unipolar CBPWM scheme. Modulation depth m is the amplitude of modulation signal u_r. The modulation depth of the adopted converter usually meets $m > 0.5$ in a steady state. If $|2\lambda - 1| \geq 0.5$, and u_r satisfies Equ. (12). In this case, switching functions S_a and S_b present dipolar characteristics, and the hybrid CBPWM operates in dipolar mode. The modulation
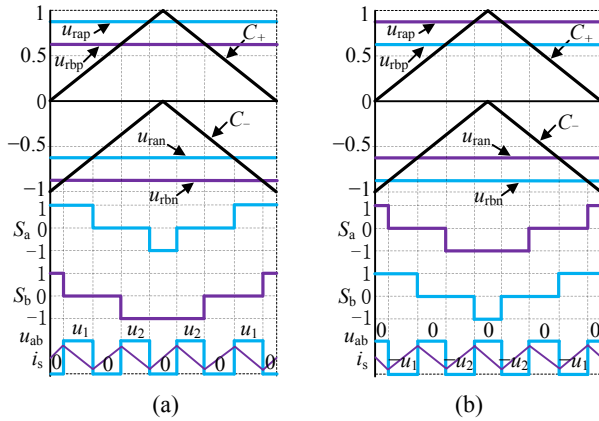
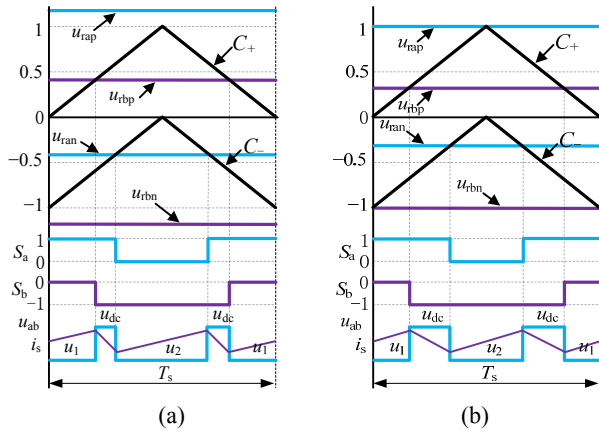Fig. 7. Hybrid CBPWM in dipolar mode. (a) $u_r > 0$. (b) $u_r < 0$.

Fig. 8. Hybrid CBPWM in unipolar mode. (a) Without compensation. (b) With compensation.

process is shown in Fig. 7. The pulse number of voltage u_{ab} in the hybrid CBPWM is twice that in the unipolar CBPWM. When the hybrid CBPWM operates in dipolar mode, the high-order harmonics caused by the hybrid CBPWM are mainly distributed around the quadruple switching frequency.

When $|u_r| \geq |2\lambda-1| \geq 0.5$, $\lambda \leq 0.25$, or $\lambda \geq 0.75$ because $|2\lambda-1| \geq 0.5$. If u_r lies in region I or region IV (Fig. 5), then u_{ab} consists of three voltage levels in one switching cycle when $\lambda \leq 0.25$. Thus, $\lambda \geq 0.75$ is chosen in the hybrid CBPWM. The modulation process is shown in Fig. 8(a).

The modulation signals u_{rap} and u_{rbn} lie in the nonlinear overmodulation region, as shown in Fig. 8(a) because $u_r \geq 2\lambda-1 \geq 0.5$ in region I and $\lambda \geq 0.75$. Assuming that $u_{rap} = 1+x$ in Fig. 8(a), we can express V_{ab} as Equ. (13), $V_{ab} \neq V_r$. The modulation algorithm in the overmodulation region does not satisfy the volt-second balance principle. Thus, a compensation algorithm shown in Equs. (14) and (15) is designed to solve this problem. The modulation process is shown in Fig. 8(b).

$$\begin{aligned} V_{ab} &= T_1 u_{dc} + 0.5T_{0.5}u_{dc} \\ &= (2u_r - 1 - x)T_s u_{dc} + (-2u_r + 2 + x)T_s 0.5 u_{dc} \\ &= (u_r - 0.5x)T_s u_{dc} \\ &\neq u_r T_s u_{dc} = V_r \end{aligned} \tag{13}$$
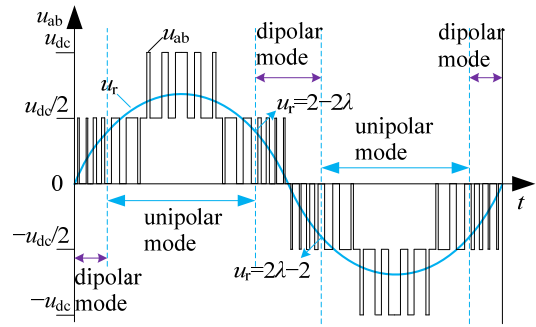

Fig. 9. Hybrid CBPWM algorithm in a complete modulation cycle.

$$\begin{cases} u_{rip} = 1 \\ u_{rin} = u_{ri} - 1 \end{cases} (u_{rip} > 1); \quad (i = a, b) \tag{14}$$

$$\begin{cases} u_{rip} = u_{ri} + 1 \\ u_{rin} = -1 \end{cases} (u_{rin} \leq -1); \quad (i = a, b) \tag{15}$$

By solving a similar triangle in Fig. 8(b) with Equs. (14) and (15), we can express V_{ab} as

$$\begin{aligned} V_{ab} &= T_1 u_{dc} + 0.5T_{0.5}u_{dc} \\ &= (2u_r - 1)T_s u_{dc} + 0.5(-2u_r + 2)T_s u_{dc} \\ &= u_r T_s u_{dc} = V_r \end{aligned} \tag{16}$$

The expression $V_{ab} = V_r$ can also be proved when u_r lies in region IV. The hybrid modulation scheme with the overmodulation compensation satisfies the volt-second balance principle. In this case, switching functions S_a and S_b present unipolar characteristics, and the hybrid CBPWM operates in unipolar mode. When the hybrid CBPWM operates in unipolar mode, the high-order harmonics caused by the hybrid CBPWM are mainly distributed around the double switching frequency.

In a complete modulation cycle, the modulated reference signal enters the overmodulation region as the magnitude of the modulated signal increases. This effect indicates that the hybrid modulation scheme switches from a dipolar mode to a unipolar mode. The unipolar mode satisfies

$$\begin{cases} u_r \geq 0 \\ u_{rap} = \dfrac{u_r}{2} + \lambda \geq 1 \\ u_{rbn} = -\dfrac{u_r}{2} - \lambda \leq -1 \end{cases} \text{ or } \begin{cases} u_r < 0 \\ u_{rbp} = -\dfrac{u_r}{2} + \lambda \geq 1 \\ u_{ran} = \dfrac{u_r}{2} - \lambda \leq -1 \end{cases} \tag{17}$$

According to the aforementioned analysis, meeting $\lambda \geq 0.75$ is necessary in the proposed hybrid CBPWM. From Equ. (17), the selection rule of operation modes in the hybrid modulation scheme can be defined as

$$\begin{cases} |u_r| \geq 2 - 2\lambda \text{ for unipolar mode} \\ |u_r| < 2 - 2\lambda \text{ for dipolar mode} \end{cases} \quad \lambda \geq 0.75 \tag{18}$$

The hybrid CBPWM algorithm in a complete modulation cycle is shown in Fig. 9. When the modulation depth m is constant, a large λ equates to a large operation range for the unipolar mode. The high-order harmonics around the
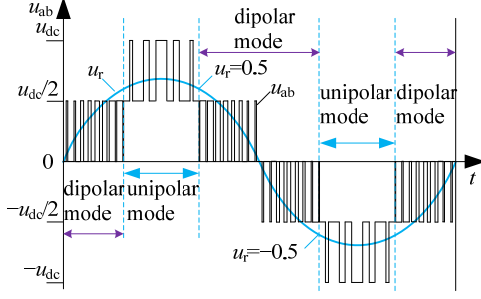
Fig. 10. Hybrid CBPWM algorithm in a complete modulation cycle at $\lambda = 0.75$.

quadruple switching frequency in dipolar mode is easier to filter and less harmful than the high-order harmonics around the double switching frequency in unipolar mode. Therefore, from the aspect of the overall high-order harmonics, $\lambda = 0.75$ is the best choice. At this point, the operation range of the dipolar mode reaches the maximum value. Fig. 10 shows the curve of voltage u_{ab} at $\lambda = 0.75$ in the hybrid CBPWM algorithm in a complete modulation cycle.

As indicated in Equ. (18), if $\lambda = 1$, $2-2\lambda = 0$, then the formula $|u_r| \geq 2-2\lambda$ is always true in a complete modulation cycle, i.e., the proposed hybrid CBPWM scheme remains in unipolar mode for all regions. The proposed hybrid CBPWM scheme is equivalent to the traditional unipolar CBPWM scheme when $\lambda = 1$.

D. Neutral-Point Voltage Balancing Control

When the hybrid CBPWM operates in unipolar mode, the neutral-point voltage balancing control method that involves injecting an offset voltage u_z into the modulation signals [7] is adopted in this work. The modified modulation signals u_{ra} and u_{rb} can be rewritten as Equ. (19).

$$\begin{cases} u_{ra} = u_r + u_z \\ u_{rb} = -u_r + u_z \end{cases} \tag{19}$$

When the hybrid CBPWM operates in dipolar mode, a similar method can be used to control the neutral-point voltage balancing. The modified modulation signals u_{rap}, u_{ran}, u_{rbp}, and u_{rbn} can be rewritten as Equ. (20). u_z is used to adjust the duty ratios of redundant states to achieve the intended neutral-point voltage balancing control.

$$\begin{cases} u_{rap} = \dfrac{u_r}{2} + \lambda + u_z \\[2mm] u_{ran} = \dfrac{u_r}{2} - \lambda - u_z \\[2mm] u_{rbp} = -\dfrac{u_r}{2} + \lambda - u_z \\[2mm] u_{rbn} = -\dfrac{u_r}{2} - \lambda + u_z \end{cases} \tag{20}$$

IV. EXPERIMENTAL RESULTS

An experimental prototype with a digital signal processor (DSP) TMS320F28335 controller is built to verify the validity

TABLE III
SYSTEM PARAMETERS

| Parameters	Value
RMS of the main voltage U_s/V	65
Grid-side inductance L/mH	5
Grid-side resistance R/Ω	0.2
DC-link support capacitor C_{dc}/mF	4.4
Load resistance R_L/Ω	60
DC-link reference voltage U_{dc}/V	170
Switching frequency f_s/kHz	1.25
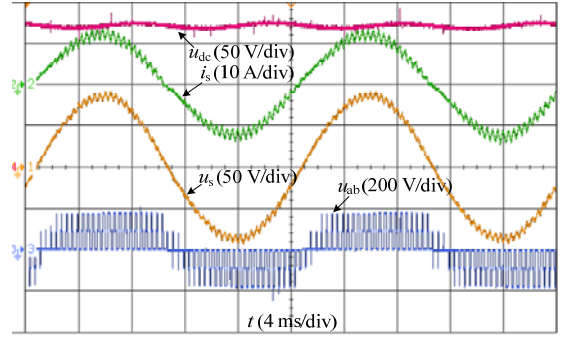
(a)
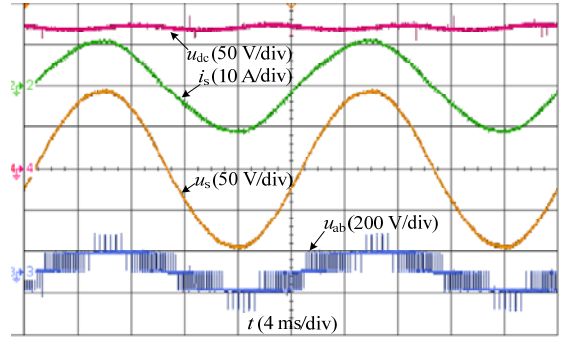
(b)

Fig. 11. Experimental waveforms of the adopted single-phase three-level converter. (a) Adopted dipolar CBPWM. (b) Proposed hybrid CBPWM.

and effectiveness of the proposed dipolar and hybrid CBPWM schemes. The parameters of the experimental system are shown in Table III.

Fig. 11(a) and (b) show the experimental waveforms of the adopted single-phase three-level converter under the proposed dipolar and hybrid CBPWM schemes, respectively. All these modulation schemes can achieve the control goals of the converter: the unit power factor and the desired constant DC-link voltage. As a result of the inductance of an autotransformer as power supply in the experimental prototype, some harmonic components can be observed in the main voltage u_s.
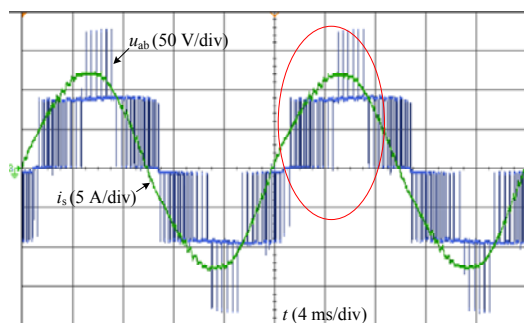
Fig. 12 present the experimental results of the line current i_s and pulse voltage u_{ab} in the adopted converter under different CBPWM schemes with the same system parameters in Table III. Different modulation schemes are adopted to achieve the same control target. Fig. 13 illustrates the enlarged view of the
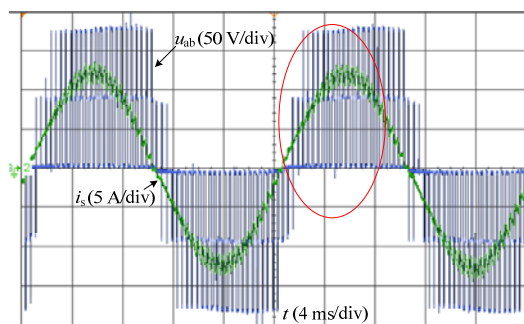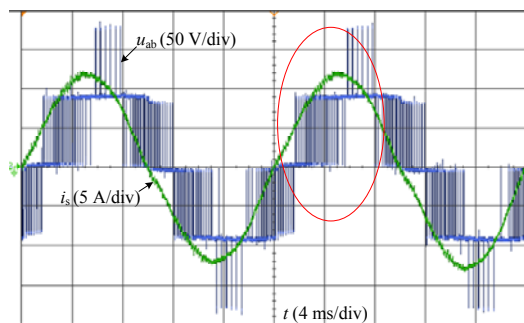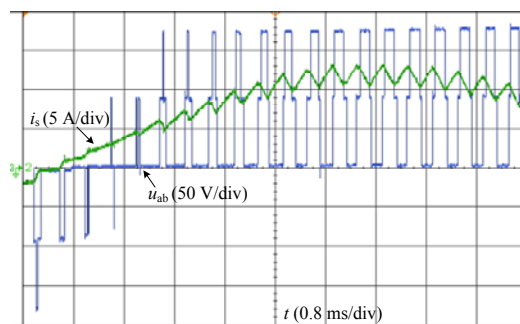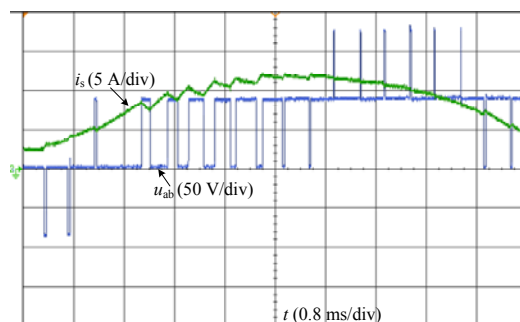
(a)
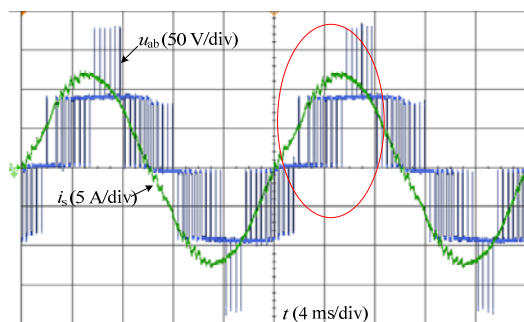
(b)

(c)

(d)

Fig. 12. Experimental results of the current i_s and voltage u_{ab} in the adopted converter. (a) Dipolar CBPWM. (b) Traditional unipolar CBPWM. (c) Proposed hybrid CBPWM at $\lambda = 0.8$. (d) Proposed hybrid CBPWM at $\lambda = 0.75$.

(a)

(b)

(c)

(d)

Fig. 13. Enlarged view of the current i_s and voltage u_{ab} in Fig. 12. (a) Dipolar CBPWM. (b) Traditional unipolar CBPWM. (c) Proposed hybrid CBPWM at $\lambda = 0.8$. (d) Proposed hybrid CBPWM at $\lambda = 0.75$.

red oval in Fig. 12 and verifies that the line current i_s changes with the pulse voltage u_{ab}. Such change is gradually reduced when the following modulation schemes are adopted: (a) dipolar CBPWM, (b) traditional unipolar CBPWM, (c) proposed hybrid CBPWM at $\lambda = 0.8$, and (d) proposed hybrid CBPWM at $\lambda = 0.75$.

The pulse voltage u_{ab} in the most modulation range consists of three voltage levels in one switching cycle when the dipolar CBPWM scheme is adopted. The variation rate of current i_s with the voltage u_{ab} step under this scheme is larger than the variation rates under the other modulation schemes. Such large variation results in an increase in the high-order harmonic

(a)

(b)

(c)

(d)
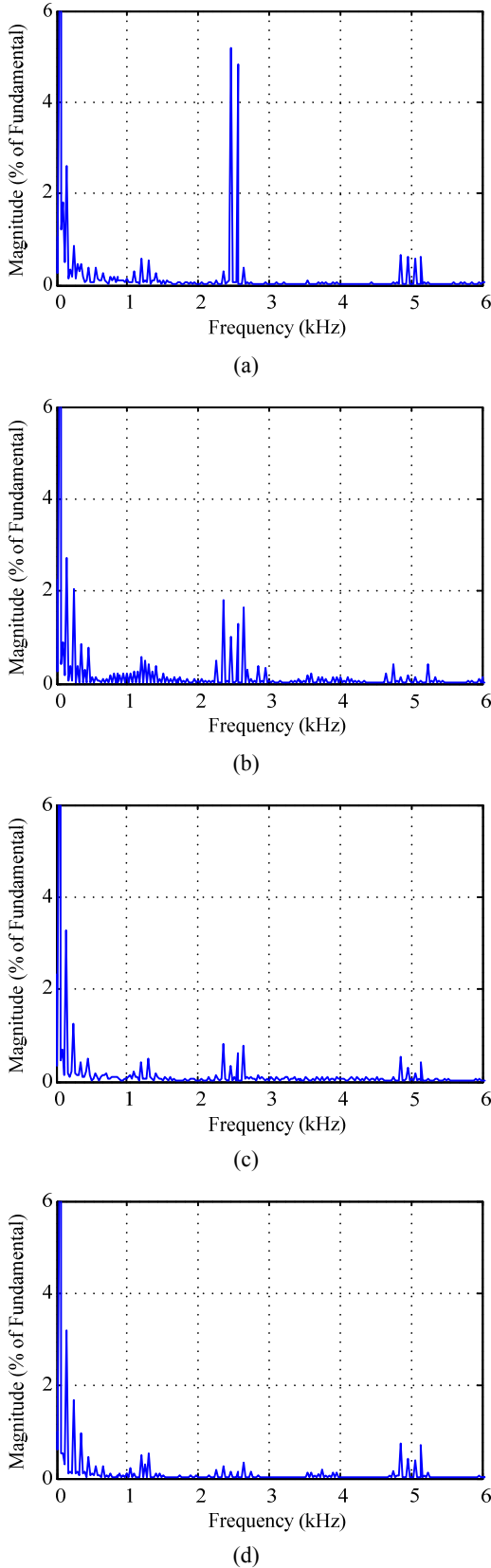
Fig. 14. FFT analysis of the experimental results for current i_s of the adopted converter. (a) Dipolar CBPWM. (b) Traditional unipolar CBPWM. (c) Proposed hybrid CBPWM at $\lambda = 0.8$. (d) Proposed hybrid CBPWM at $\lambda = 0.75$.
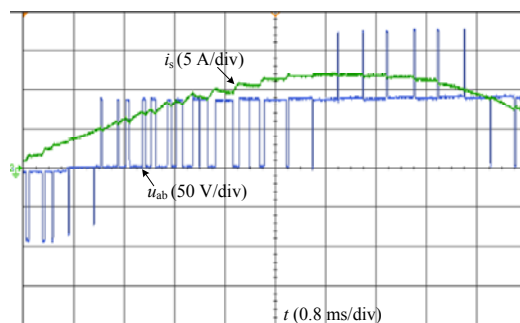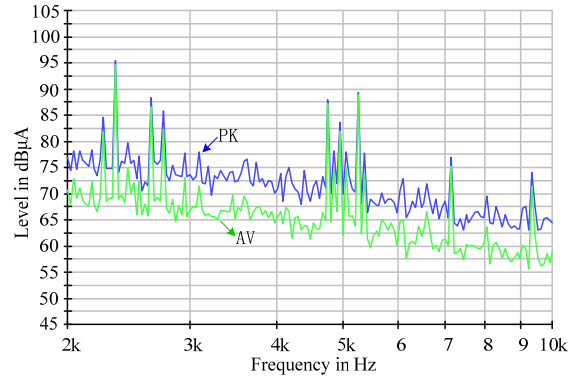

Fig. 15. EMI experimental results of the traditional unipolar CBPWM scheme.
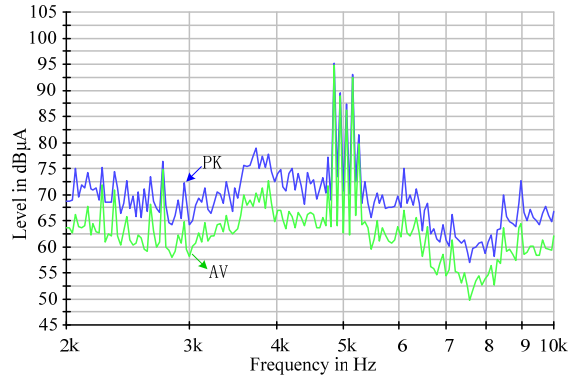
Fig. 16. EMI experimental results of the proposed hybrid CBPWM scheme.

components of the dipolar CBPWM scheme. In the same switching frequency, the proposed hybrid CBPWM scheme increases the pulse number of voltage u_{ab} in comparison with the traditional unipolar CBPWM scheme. The coefficient λ is in the range of $0.75 \leq \lambda \leq 1$; a small coefficient λ equates to a large number of pulses and to minimal line current ripples.

Fig. 14 shows the fast Fourier transform (FFT) analysis results of the line current i_s in Fig. 12. The high-order harmonic components of the line current are gradually reduced when the following modulation schemes are adopted: (a) dipolar CBPWM, (b) traditional unipolar CBPWM, (c) proposed hybrid CBPWM at $\lambda = 0.8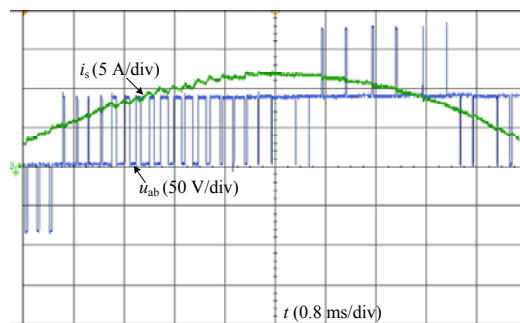$, and (d) proposed hybrid CBPWM at $\lambda = 0.75$. The control delay interval caused by the loading modulation signal u_r spans one switching cycle in the DSP controller. Hence, the modulation signal u_r is discretized with the switching frequency f_s. Thus, the line current i_s contains the harmonic components distributed around the switching frequency ($f_s = 1.25$ kHz).

The experimental results in Figs. 12–14 verify the validity of the aforementioned analysis. The high-order harmonic components of current i_s are the largest when the dipolar CBPWM scheme is adopted. The proposed hybrid CBPWM scheme can reduce the high-order harmonics around the double switching frequency. The comparison of Figs. 14(c) and 14(d) shows that a small λ equates to low high-order harmonic

components in the range of $\lambda \geq 0.75$. These experimental results verify that the high-order harmonic components can reach the minimum value at $\lambda = 0.75$, which coincides with the abovementioned theoretical analysis results.

Fig. 15 and Fig. 16 show the conducted EMI experimental results of the traditional unipolar CBPWM scheme and the proposed hybrid CBPWM scheme at $\lambda = 0.75$, respectively. The blue line represents the peak detector (PK), and the green line denotes the average detector (AV). Fig. 15 and Fig. 16 also indicate that the large EMI noises are distributed around the double switching frequency (2.5 kHz) and quadruple switching frequency (5 kHz) when the traditional unipolar CBPWM scheme is adopted. The large EMI noises are only distributed around the quadruple switching frequency (5 kHz) when the proposed hybrid CBPWM scheme is adopted. However, the maximum EMI noise can reach 95 dBμA, which is the same as that in the traditional unipolar CBPWM scheme. Nevertheless, the proposed method can transfer the EMI noise around the double switching frequency (2.5 kHz) to the quadruple switching frequency (5 kHz).

V. CONCLUSION

A single-phase three-level dipolar CBPWM scheme is designed in this work. On the basis of the dipolar CBPWM scheme, a novel hybrid CBPWM scheme that combines unipolar and dipolar modulations is proposed. Unlike the traditional unipolar CBPWM scheme, the proposed dipolar and hybrid CBPWM schemes have the following salient features.

1) In the dipolar CBPWM scheme, the switching function of each leg is dipolar in each switching cycle when u_r lies in the complete modulation range. The pulse voltage u_{ab} comprises three voltage levels in each switching cycle when u_r lies in the most modulation range.

2) The dipolar CBPWM scheme increases the high-order harmonic components distributed around the double switching frequency.

3) The hybrid CBPWM scheme consists of two modulation modes in the complete modulation range. In dipolar mode, the switching function of each leg is dipolar with three states (1 0 −1) in one switching cycle. Otherwise, they are unipolar with two states (0 1, or 0 −1) in unipolar mode. However, the pulse voltage u_{ab} consists of two voltage levels in one switching cycle in both dipolar and unipolar modes.

4) The hybrid CBPWM scheme can transfer the harmonics and EMI noises around the double switching frequency to the quadruple switching frequency and reduce the high-order harmonic components. The hybrid CBPWM scheme can reach the best status at a separation coefficient of $\lambda = 0.75$.

5) The hybrid CBPWM scheme can effectively utilize the switching frequency at the same heat sink design of the switching loss and reduce the probability of harmonic resonance accidents in electric railway traction systems.

REFERENCES

[1] R. Gonzalez, E. Gubia, J. Lopez, and L. Marroyo, "Transformerless single-phase multilevel-based photovoltaic inverter," *IEEE Trans. Ind. Electron.*, Vol. 55, No. 7, pp. 2694-2702, Jul. 2008.

[2] V. Minambres-Marcos, E. Romero-Cadaval, M. A. Guerrero-Martinez, and M. I. Milanes-Montero, "Cooperative converter for improving the performance of grid-connected photovoltaic power plants," *IET Renew. Power Gener.*, Vol. 7, No. 2, pp. 110-117, Mar. 2013.

[3] C. Lin, C. Young, W. Yeh, and Y. Liu, "An LVRT control strategy for reducing DC-link voltage fluctuation of a two-stage photovoltaic multilevel inverter," in *Proc. IEEE 10th PEDS Conf.*, pp. 908-913, 2013.

[4] J. A. Heerdt, J. A. Heerdt, S. A. Mussa, S. A. Mussa, M. L. Heldwein, and M. L. Heldwein, "Semiconductors current efforts and losses evaluation for single-phase three-level regenerative PWM rectifiers," in *Proc. IEEE ISIE Conf.*, pp. 1046-1051, 2010.

[5] M. Narimani and G. Moschopoulos, "A new single-phase single-stage three-level power factor correction AC–DC converter," *IEEE Trans. Power Electron.*, Vol. 27, No. 6, pp. 2888-2899, Jun. 2012.

[6] P. M. Barbosa, F. Canales, J. M. Burdio, and F. C. Lee, "A three-level converter and its application to power factor correction," *IEEE Trans. Power Electron.*, Vol. 20, No. 6, pp. 1319-1327, Nov. 2005.

[7] W. Song, X. Feng and K. M. Smedley, "A carrier-based PWM strategy with the offset voltage injection for single-phase three-level neutral-point-clamped converters," *IEEE Trans. Power Electron.*, Vol. 28, No. 3, pp. 1083-1095, Mar. 2013.

[8] G. W. Chang, H. W. Lin and S. K. Chen, "Modeling characteristics of harmonic currents generated by high-speed railway traction drive converters," *IEEE Trans. Power Del.*, Vol. 19, No. 2, pp. 766-773, Apr. 2004.

[9] W. Song, S. Wang, C. Xiong, X. Ge, and X. Feng, "Single-phase three-level space vector pulse width modulation algorithm for grid-side railway traction converter and its relationship of carrier-based pulse width modulation," *IET Electr. Syst. Transp.*, Vol. 4, No. 3, pp. 78-87, Sep. 2014.

[10] H. Hu, Z. He, and S. Gao, "Passive filter design for china High-Speed railway with considering harmonic resonance and characteristic harmonics," *IEEE Trans. Power Del.*, Vol. 30, No. 1, pp. 505-514. Feb. 2015.

[11] H. Cui, W. Song, H. Fang, X. Ge, and X. Feng, "Resonant harmonic elimination pulse width modulation-based high-frequency resonance suppression of high-speed

railways," *IET Power Electron.*, Vol. 8, No. 5, pp. 735-742, Oct. 2014.

[12] M. Brenna and F. Foiadelli, "Analysis of the filters installed in the interconnection points between different railway supply systems," *IEEE Trans. Smart Grid*, Vol. 3, No. 1, pp. 551-558, Mar. 2012.

[13] Z. He, H. Hu, Y. Zhang, and S. Gao, "Harmonic resonance assessment to traction power-supply system considering train model in china high-speed railway," *IEEE Trans. Power Del.*, Vol. 29, No. 4, pp. 1735-1743. Aug. 2014.

[14] A. Iagar, G. N. Popa and I. Sora, "Analysis of electromagnetic pollution produced by line frequency coreless induction furnaces," *WSEAS Trans. Syst.*, Vol. 8, No. 1, pp. 1-11, Jan. 2009.

[15] J. Liu, Q. Yang and T. Q. Zheng, "Harmonic analysis of traction networks based on the CRH380 series EMUs accident," in *Proc. IEEE ITEC Conf.*, pp. 1-6, 2012.

[16] S. Eren, M. Pahlevani, A. Bakhshai, and P. Jain, "An adaptive droop DC-bus voltage controller for a grid-connected voltage source inverter with LCL filter," *IEEE Trans. Power Electron.*, Vol. 30, No. 2, pp. 547-560, Feb. 2015.

[17] J. Yin, S. Duan and B. Liu, "Stability analysis of grid-connected inverter with LCL filter adopting a digital single-loop controller with inherent damping characteristic," *IEEE Trans. Ind. Inf.*, Vol. 9, No. 2, pp. 1104-1112, May 2013.

[18] S. Liang, Q. Hu and W. J. Lee, "A survey of harmonic emissions of a commercially operated wind farm," *IEEE Trans. Indus. Appl.*, Vol. 48, No. 3, pp. 1115-1123, May-Jun. 2012.

[19] O. Husev, A. Chub, E. Romero-Cadaval, C. Roncero-Clemente, and D. Vinnikov, "Voltage distortion approach for output filter design for off-grid and grid-connected PWM inverters," *Journal of Power Electrons*, Vol. 15, No. 1, pp. 278-287, Jan. 2015.

[20] Z. Zhao, Y. Zhong, H. Gao, L. Yuan, and T. Lu, "Hybrid selective harmonic elimination PWM for common-mode voltage reduction in three-level neutral-point-clamped inverters for variable speed induction drives," *IEEE Trans. Power Electron.*, Vol. 27, No. 3, pp. 1152-1158, Mar. 2012.

[21] M. Balasubramonian and V. Rajamani, "Design and real-time implementation of SHEPWM in single-phase inverter using generalized hopfield neural network," *IEEE Trans. Ind. Electron.*, Vol. 61, No. 11, pp. 6327-6336, Nov. 2014.

[22] A. V. Stankovic and C. Ke, "A new control method for input-output harmonic elimination of the PWM boost-type rectifier under extreme unbalanced operating conditions," *IEEE Trans. Ind. Electron.*, Vol. 56, No. 7, pp. 2420-2430, Jul. 2009.

[23] K. Song, M. Wu, V. G. Agelidis, and H. Wang, "Line current harmonics of three-level neutral-point-clamped electric multiple unit rectifiers: analysis, simulation and testing," *IET Power Electron.*, Vol. 7, No. 7, pp. 1850-1858, Jul. 2014.

[24] F. A. Ramirez and M. A. Arjona, "Development of a grid-connected wind generation system with a modified PLL structure," *IEEE Trans. Sustain. Energy*, Vol. 3, No. 3, pp. 474-481, Jul. 2012.

[25] J. Salaet, A. Gilabert, J. Bordonau, S. Alepuz, A. Cano, and L. M. Gimeno, "Nonlinear control of neutral point in three-level single-phase converter by means of switching redundant states," *Electron. Lett.*, Vol. 42, No. 5, pp. 304-306, Mar. 2006.

[26] K. Paiboon and S. Somboon, "A unified PWM method for matrix converters and its carrier-based realization using dipolar modulation technique", *IEEE Trans. Ind. Electron.*, Vol. 59, No. 1, pp. 80-92, Jan. 2012.

[27] N. Li, Y. Wang, W. Lei, R. Niu, and Z. Wang, "Novel carrier-based PWM strategy of a three-level NPC voltage source converter without low-frequency voltage oscillation in the neutral point," *Journal of Power Electrons*, Vol. 14, No. 3, pp. 531-540, May 2014.

Shunliang Wang was born in Sichuan, China, in 1987. In 2010, he received his B.S. degree in Electrical Engineering from Southwest Jiaotong University, Chengdu, China, where he is currently working toward his Ph.D. degree in Electrical Engineering. His current research interests include digital control and modulation of power converters, multilevel converters, and power electronic transformers in railway applications.

Wensheng Song received his B.S. degree in Electronic and Information Engineering and his Ph.D. degree in Electrical Engineering from Southwest Jiaotong University, Chengdu, China, in 2006 and 2011, respectively. He is currently a Lecturer in the School of Electrical Engineering, Southwest Jiaotong University. From September 2009 to September 2010, he was a Visiting Scholar at the Department of Electrical Engineering and Computer Science, University of California, Irvine, CA, USA. From July 2015 to December 2015, he was a Visiting Scholar at the University of Alberta, Edmonton, Canada. His current research interests include digital control and modulation methods for electrical ac–dc–ac railway traction drive systems and multilevel converters.

Xiaoyun Feng received her B.S., M.S., and Ph.D. degrees in Electrical Engineering from Southwest Jiaotong University, Chengdu, China, in 1983, 1988, and 2001, respectively. Since 1983, she has been with the School of Electrical Engineering, Southwest Jiaotong University, where she is currently a full Professor. She was a Visiting Professor at the University of Tokyo between October 1998 and October 1999. She is the author or coauthor of more than 70 papers. Her main research interests include the analysis and control of electrical traction converters and motor drive systems, design of railway traction characteristics, and railway train optimizing operations.

Rongjun Ding received his B.S. degree in Electrical Engineering from Southwest Jiaotong University, Chengdu, China, in 1984, and his M.S. and Ph.D. degrees in Traffic Signal and Control Engineering from Central South University, Changsha, China, in 1998 and 2008, respectively. He is a Fellow of the China Academy of Engineering (FCAE). Since 2011, he has been a professor in the School of Electrical Engineering, Southwest Jiaotong University. His main research interests include the control of electrical traction converters and motor drive systems and network control technology in railway applications.